JFM RAPIDS
journals.cambridge.org/rapids

A multifractal model for the momentum transfer process in wall-bounded flows

X. I. A. Yang[1,†] **and A. Lozano-Durán**[1]

[1]Center for Turbulence Research, Stanford, 94305, USA

The cascading process of turbulent kinetic energy from large-scale fluid motions to small-scale and lesser-scale fluid motions in isotropic turbulence may be modelled as a hierarchical random multiplicative process according to the multifractal formalism. In this work, we show that the same formalism might also be used to model the cascading process of momentum in wall-bounded turbulent flows. However, instead of being a multiplicative process, the momentum cascade process is additive. The proposed multifractal model is used for describing the flow kinematics of the low-pass filtered streamwise wall-shear stress fluctuation τ'_l, where l is the filtering length scale. According to the multifractal formalism, $\langle \tau'^2 \rangle \sim \log(Re_\tau)$ and $\langle \exp(p\tau_l) \rangle \sim (L/l)^{\zeta_p}$ in the log-region, where Re_τ is the friction Reynolds number, p is a real number, L is an outer length scale and ζ_p is the anomalous exponent of the momentum cascade. These scalings are supported by the data from a direct numerical simulation of channel flow at $Re_\tau = 4200$.

1. Introduction

The phenomenological explanation of the transfer of turbulent kinetic energy from large to small scales was introduced in the classical paper by Kolmogorov (1941) (from now on K41) but the concept of a turbulent cascade in terms of interactions among eddies was proposed earlier by Richardson (1922), and later by Obukhov (1941). Since then, many detailed investigations, mostly in isotropic turbulence (HIT), have greatly advanced our understanding of high-Reynolds-number turbulent flows (Onsager 1949; Batchelor 1953; Heisenberg 1985; Mandelbrot 1999; Jiménez 2012), with some of them even testing the original idea of Richardson (1922) in terms of eddies merging and splitting as in Lozano-Durán & Jiménez (2014*b*).

There have been many different attempts to unravel the physical mechanism behind the cascade with varying but complementary tools. A classic physical explanation is

† Email address for correspondence: xiangyang@stanford.edu

given in terms of vortex stretching, where the strain at a given scale stretches vortices at a smaller scale. This interaction induces higher velocities by the conservation of angular momentum, resulting in a net energy transfer from large to small scales (Goto 2012; Leung, Swaminathan & Davidson 2012; Lozano-Durán, Holzner & Jiménez 2016). It has also been known for some time that the cascade is not one-directional from large to small scales, but that there is a balance between direct and inverse transfers. Most of the evidence for this backscatter originates from filtering techniques in scale space (Piomelli *et al.* 1991; Aoyama *et al.* 2005; Cardesa *et al.* 2015). Other interpretations of the cascade are rooted in statistical mechanics, as the works by Leith (1967) and Orszag (1970), where energy transfer is modelled as an entropy-driven random process in phase space, with the energy tending to equipartition while drifting either up or down in scale.

In the present work, we focus on the multifractal formalism (Meneveau & Sreenivasan 1991; Frisch & Donnelly 1996; Mandelbrot 1999), which has been successful in characterizing the inertial energy cascade. Within this framework, statistical properties of the flow such as the central moments of the two-point velocity increments and the coarse-grained energy dissipation have been reasonably well estimated. However, instead of energy, here we will study another often-encountered cascading process in wall-bounded turbulence, that is, the momentum. In this case, momentum is transferred from the large energy-containing eddies to smaller scales until it is drained at the wall.

The momentum cascade and the energy cascade are, in many ways, analogous. The sizes of the energy-containing motions are the only relevant length scales in the inertial range; consequently, the energy flux is nearly constant across all scales in the inertial range. The analogous range of scales in wall-bounded flows is the logarithmic range. In the log-region, eddy sizes scale with their distance from the wall and the momentum flux $-\langle u'v'\rangle$ is almost constant, where u, v are the velocities in the streamwise and wall-normal directions, the superscript $\prime$ indicates fluctuating quantities and $\langle\cdot\rangle$ denotes ensemble average. Fluid motions in the inertial range are self-similar, as is also the case for structures in the log-region (see e.g. Del Álamo *et al.* 2006; Lozano-Durán, Flores & Jiménez 2012; Marusic *et al.* 2013; Baars, Hutchins & Marusic 2017; Morrill-Winter, Philip & Klewicki 2017), consistent with the attached-eddy hypothesis scenario proposed by Townsend (1980) and extended by Perry & Chong (1982) and Marusic & Perry (1995). Dissipation drains energy at viscous scales $(\nu^3/\langle\epsilon\rangle)^{1/4}$, where ν is the kinematic viscosity and ϵ is the energy dissipation. Momentum, on the other hand, is drained at the wall by fluid motions of viscous scales $\sim\nu/u_\tau$, where u_τ is the friction velocity. Both dissipation and wall-stress fluctuations are known to be intermittent (see e.g. Park *et al.* (2012) and Mathis *et al.* (2013) for discussion on the wall-stress fluctuations).

Despite the many common features, four decades after the work of Mandelbrot (1972), the multifractal formalism has not been extended to modelling of the momentum cascade in wall-bounded flows. Even the basic idea of momentum cascade has not been used as much as its energy counterpart by the wall-bounded turbulence community (see e.g. Flores & Jiménez (2010) and Jiménez (2012) for some discussion on the difference and common features between the momentum cascade and the energy cascade).

In the present work, the momentum cascade in wall-bounded flows at high Reynolds numbers is investigated using the multifractal framework. A brief introduction to the multifractality is included in § 2. In § 3, an analogy is formally made between the energy cascade and the momentum cascade. The multifractal formalism is then
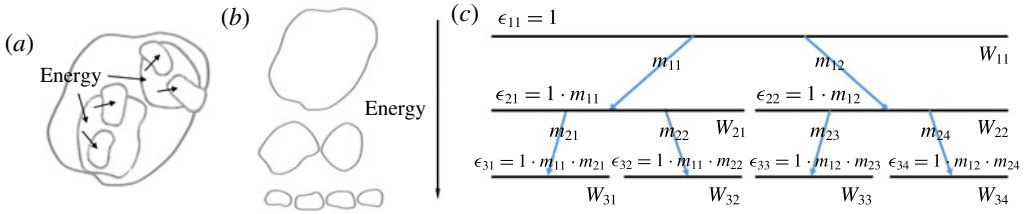
FIGURE 1. (*a*) A sketch of the Richardson cascade. (*b*) A typical sketch of the Richardson cascade in textbooks. Eddies of different sizes are displaced. (*c*) A schematic of the energy cascade according to the multifractal formalism. ϵ_{nj} is the volume-averaged dissipation rate in eddy W_{nj}. m_{nj} is a multiplicative. W_{11} is the first of the hierarchy. Three hierarchies are sketched.

extended to modelling the momentum cascade. Estimates of the scalings of the low-pass filtered wall-shear stress are presented and tested in a direct numerical simulation (DNS) of channel flow at friction Reynolds number $Re_\tau = 4200$. Finally, a short discussion and summary are given in § 4.

2. The energy cascade and the multifractal formalism

The cascade process of Richardson (1922) is sketched in figure 1. In such sketches, eddies of different sizes are often displaced for illustration purposes, as is done in figure 1(*b*) (see e.g. Frisch & Donnelly 1996; Pope 2001).

Developments after the celebrated K41 phenomenology have led to the fractal and multifractal formalism (see Frisch & Donnelly 1996) as well as Navier–Stokes-based statistical models including the direct interaction approximation and the shell model (Kraichnan 1991, 1965; Biferale 2003). The discussion in this section is limited to multifractal models. Figure 1(*c*) is a schematic of the cascade process according to the multifractal formalism. We define the volume-averaged energy transfer (including both forward cascading and backward scattering) in an eddy W_{nj} as

$$\Pi_{nj} = \frac{1}{V_{nj}} \int_{W_{nj}} \Pi \, \mathrm{d}V, \tag{2.1}$$

where V_{nj} is the volume of eddy W_{nj}, and the subscript n and j indicate the jth eddy at the nth cascade step, respectively. Without loss of generality, $\Pi_{11} = 1$. Analogously the volume-averaged dissipation rate is defined as

$$\epsilon_{nj} = \frac{1}{V_{nj}} \int_{W_{nj}} \epsilon \, \mathrm{d}V. \tag{2.2}$$

For statistically stationary flows, $\langle \epsilon_{nj} \rangle = \langle \Pi_{nj} \rangle$ by energy conservation. When W_{11} breaks into W_{21}, W_{22}, the energy flux is not necessarily equally split into the daughter eddies. The volume-averaged dissipation rates in W_{21} and W_{22} are therefore not 1 in general. Without loss of generality, in eddy W_{21}, $\epsilon_{21} = 1 \cdot m_{12}$ and in eddy W_{22}, $\epsilon_{22} = 1 \cdot m_{22}$. According to figure 1(*a*), $\epsilon_{21}V_{21} + \epsilon_{22}V_{22} = \epsilon_{11}V_{11}$. This cascade process continues, giving rise to eddy W_{3j} and fluid motions of lesser sizes.

After n steps of this cascade process, the size of the energy-containing eddies decreases to $l = L/r^n$, where L is the characteristic length of eddy W_{11} and r

is a constant. Following Meneveau & Sreenivasan (1991), r is set to be 2. The volume-averaged dissipation rate in eddy W_{nj} is

$$\epsilon_{nj} = 1 \cdot m_{1j_1} \cdot m_{2j_2} \ldots \cdot m_{nj_n}, \qquad (2.3)$$

where $j_1, j_2, \ldots, j_n$ are indices of the multiplicatives at the 1st, 2nd, and nth cascade step that lead to W_{nj}. According to (2.3), the energy cascade is a multiplicative process and only interactions among neighbouring scales are accounted for. For $l = L/r^n$ in the inertial range, the cascade process is self-similar and m_{ij}'s are identically distributed multiplicatives and equal to m. Then, equation (2.3) leads to the following scaling laws

$$\langle (\epsilon_n/\epsilon_1)^p \rangle \sim \langle m^p \rangle^n \sim (L/l)^{\zeta_p}, \quad \zeta_p = \log_2(\langle m^p \rangle), \qquad (2.4)$$

where the eddy index j is dropped, ϵ_n is the volume-averaged energy dissipation of a typical eddy at the nth cascade step and $p > 0$ is an integer. ζ_p is the so-called 'anomalous exponent'. According to K41, the energy flux is equally split into the daughter eddies at every cascade step, which implies $m \equiv 1$ and $\langle \epsilon_l^p \rangle = \langle \epsilon_1 \rangle^p$. Later, Kolmogorov (1962) modelled $\log(m)$ as a Gaussian random variable. According to this log-normal model, $\zeta_p = c_1 p^2 + c_2 p$, where c_1, c_2 are constants. The reader is directed to Frisch & Donnelly (1996) for detailed discussions on other fractal and multifractal models including the β model (Frisch, Sulem & Nelkin 1978), the p-model (Meneveau & Sreenivasan 1987), etc. The brief overview here is merely a short introduction to the basic ideas behind the multifractal formalism and is not meant to be a comprehensive review of the work on the topic of energy cascade.

3. The momentum cascade

Figure 2 is a schematic of the momentum cascade in high-Reynolds-number wall-bounded turbulence. The streamwise momentum is carried by the large-scale eddies in the boundary layer, then passed to small-scale and lesser-scale eddies and last drained at the wall. The momentum transfer in wall turbulence is governed by the flux term $(-\langle u(v + V_r) \rangle + \nu \partial u/\partial y)$, where V_r is the wall-normal velocity of the frame of reference. Although it is the wall-normal derivative of the flux term that enters the momentum equation, whose sign is independent of the frame of reference, the sign of the flux term itself does depend on V_r (Jiménez 2016). To avoid ambiguity, we consider the momentum cascade of the fluctuating velocities in this study, as is usually done for the energy cascade in HIT. In this case, the mean velocity does not play a role, and the direction of the momentum transfer is determined by the flux term $\langle u'v' \rangle$, which is independent of the frame of reference. In wall-bounded flows, where positive y is the wall-normal direction and points away from the wall, u' and v' are negatively correlated on average. This determines the momentum transfer, on average, being from the bulk region to the wall. Unless noted otherwise, wall units are used for normalization.

The quantity of interest here is the low-pass filtered streamwise wall-stress fluctuation, which is defined as

$$\tau_l'(\boldsymbol{x}) = \int G_l(\boldsymbol{x} - \boldsymbol{r}) \tau'(\boldsymbol{r}) \, \mathrm{d}\boldsymbol{r}, \qquad (3.1)$$

where τ is the wall-shear stress in the flow direction, G_l is a filtering kernel, and the subscript l is the filtering length scale. $\tau_l' = 0$ for $l/\delta \to \infty$ and $\tau_l' = \tau'$ for $l/(\nu/u_\tau) \to 0$.
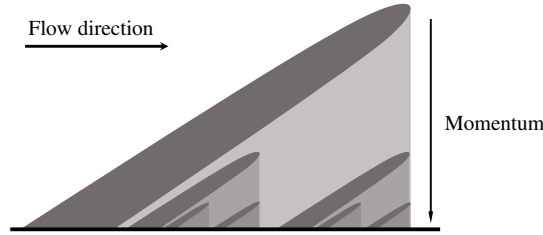
FIGURE 2. A schematic of the momentum cascade from large-scale eddies to small-scale eddies in wall-bounded flows. The shear stresses on the wall bear footprints of eddies of all scales (lightly shaded grey).

We model the low-pass filtered wall-stress fluctuation as an additive process (see Yang, Marusic & Meneveau 2016*a*, for other flow quantities that follow additive processes)

$$\tau'_l(x, z) = a_1(x, z) + a_2(x, z) + a_3(x, z) + \cdots + a_{n_l}(x, z), \tag{3.2}$$

where both τ'_l and the addends a_i are functions of spatial coordinates at the wall (x and z), an addend a_i is an increment in τ'_l due to an eddy of height $\sim \delta/2^i$. δ is the boundary layer height and the number of addends is $n_l \sim \log_2(\delta/l)$. The spatial dependence will be dropped hereafter for brevity. Following the multifractal formalism, the addends a_i are identically and independently distributed (i.i.d.) and equal to a. Filtering at the viscous scale $\sim \nu/u_\tau$ gives back the unfiltered wall-shear stress $\tau' = \tau'_{C\nu/u_\tau}$, where C is an $O(1)$ constant. According to (3.2), the variance of the wall-shear stress fluctuations in boundary layer flows follows

$$\langle \tau'^2 \rangle = \langle \tau'^2_{C\nu/u_\tau} \rangle = \langle (a_1 + a_2 + \cdots + a_{n_{C\nu/u_\tau}})^2 \rangle = \langle a_1^2 \rangle + \langle a_1^2 \rangle + \cdots + \langle a_{n_{C\nu/u_\tau}}^2 \rangle$$
$$= n_{C\nu/u_\tau} \langle a^2 \rangle \sim \log(\delta/(C\nu/u_\tau)) \sim \log(Re_\tau), \tag{3.3}$$

where $\langle a_i a_j \rangle = 0$ for $i \neq j$. It then follows that STD $(\tau') \equiv \sqrt{\langle \tau'^2 \rangle} \sim \sqrt{\log(Re_\tau)}$. This is in contrast to the scaling suggested by Schlatter & Örlü (2010)

$$\sqrt{\langle \tau'^2 \rangle} \sim \log(Re_\tau), \tag{3.4}$$

and the one proposed by Alfredsson *et al.* (1988), STD $(\tau') = 0.4$. Figures 3(*a,b*) show respectively the standard deviation and the variance of the wall-shear stress fluctuations in boundary layer flows as functions of the friction Reynolds number. Both scalings in (3.3), (3.4) provide reasonably good fits for the data from low to moderate Reynolds numbers. Considering this, including DNS data, which are between $Re_\tau \approx 180$ (Kim, Moin & Moser 1987) and $Re_\tau \approx 5200$ (Lee & Moser 2015) is not very useful here. Predictions according to (3.3), (3.4) are only tellingly different at high Reynolds numbers ($Re_\tau > 10^5$), where only one data point is available. The available data generally favour (3.3). The evidence here, however, is not conclusive, because the data from Mathis *et al.* (2013) are not direct measurements but are inferred results based on a calibrated near-wall small-scale signal and a modulation model. Future confirmation/refutation of the scaling in (3.3) will need measurements of the wall-shear stresses from one same facility at friction Reynolds numbers that span at least two decades (from $Re_\tau \approx 10^3$ to 10^5 and higher), an investigation that may be done at CICLoPE (Vinuesa, Duncan & Nagib 2016).
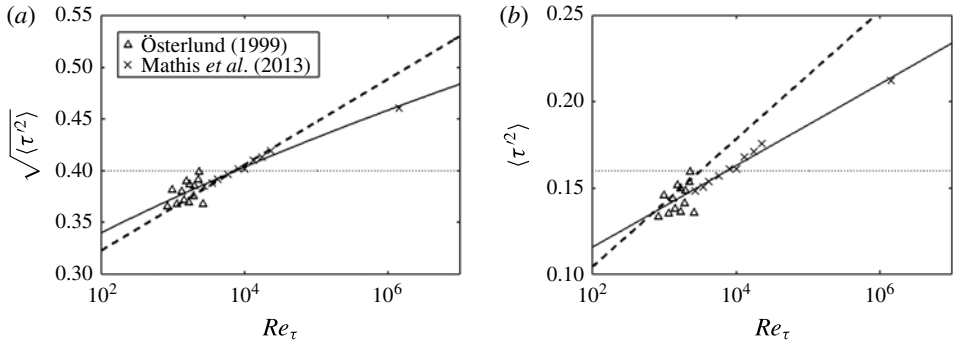
FIGURE 3. (*a*) $\sqrt{\langle \tau'^2 \rangle}$ as a function of Re_τ. The data are reported in Österlund (1999) and Mathis *et al.* (2013). The dotted line corresponds to $\sqrt{\langle \tau'^2 \rangle} = 0.4$ from Alfredsson *et al.* (1988). The dashed line corresponds to the scaling $\sqrt{\langle \tau'^2 \rangle} = 0.24 + 0.018 \ln(Re_\tau)$ (Schlatter & Örlü 2010). The solid line is the least-square fit of the data according to (3.3) and is $\langle \tau'^2 \rangle = 0.10 + 0.68 \ln(Re_\tau)$. (*b*) $\langle \tau'^2 \rangle$ as a function of Re_τ. The dashed line and the solid line are straight lines in (*a*) and (*b*), respectively.
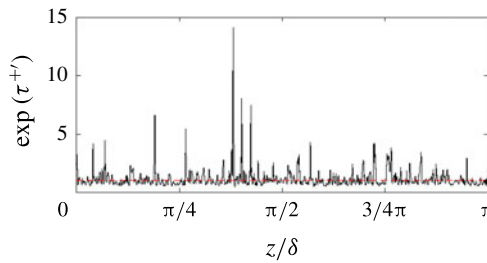

FIGURE 4. $\exp(\tau')$ as a function of the spanwise coordinate in channel flow at $Re_\tau = 4200$. The dashed line corresponds to $\tau' = 0$.

It is worth noting that according to (3.2), $\exp(\tau'_l)$ follows a multiplicative process. Therefore $\exp(\tau'_l)$ is formally analogous to the energy dissipation rate in HIT. Figure 4(*a*) shows $\exp(\tau')$ as a function of the spanwise coordinate. The signal resembles dissipation signals in HIT (see e.g. figure 1(*b*) in Meneveau & Sreenivasan (1991) for comparison). The data are from the DNS of Lozano-Durán & Jiménez (2014*a*) of channel flow at $Re_\tau \approx 4200$.

We have examined $\langle \tau'^2 \rangle$ as a function of the friction Reynolds number in figure 3 and $\exp(p\tau')$ qualitatively in figure 4. Next, we investigate the scaling behaviour of the moment generating function $\langle \exp(p\tau'_l) \rangle$, which is a useful statistical tool in general and central moments can be derived by $\langle \phi^n \rangle = d\langle \exp(p\phi) \rangle / dp|_{p=0}$, where ϕ is a generic random statistical quantity. To make predictions of the scaling behaviour of $\langle \exp(p\tau'_l) \rangle$ as a function of l, we follow the same steps that lead to (2.4). Considering addends being i.i.d.,

$$
\begin{aligned}
\langle \exp(p\tau'_l) \rangle &\sim \langle \exp(pa_1) \rangle \langle \exp(pa_2) \rangle \langle \exp(pa_3) \rangle \cdots \langle \exp(pa_{n_l}) \rangle \\
&\sim \langle \exp(pa) \rangle^{n_l} \sim (\delta/l)^{\log_2(\langle \exp(pa) \rangle)} \\
&= (\delta/l)^{\zeta_p}, \quad \zeta_p = \log_2(\langle \exp(pa) \rangle).
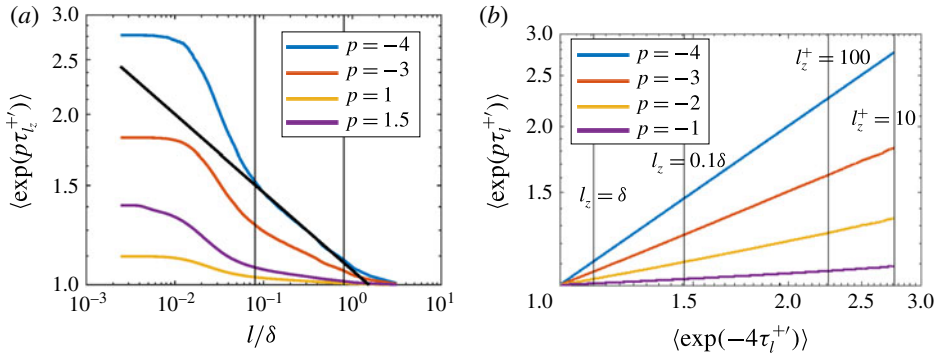\end{aligned} \tag{3.5}
$$

FIGURE 5. (a) $\langle\exp(p\tau'_l)\rangle$ as functions of the filtering length for $p = -4$, -3, 1, 1.5. The enclosed region corresponds to $340 < l_z^+$ and $l/\delta < 0.8$. The stress is low-pass filtered in the spanwise direction. The bold line indicates the slope of $\langle\exp(-4\tau'_l)\rangle$ in the enclosed region and the slope is 0.14. (b) $\langle\exp(p\tau'_l)\rangle$ as functions of $\langle\exp(-4\tau'_l)\rangle$ for $p = -4$, -3, -2, -1. The corresponding values of the reference scaling at $l = \delta$, 0.1δ and $l^+ = 100$, 10 are indicated using thin vertical lines.

While isotropy is expected at small scales in the bulk region (at scales $\ll y$, see Saddoughi & Veeravalli (1994) for detailed discussion), at the wall, isotropy is not expected at any scale because of the dominating effect of shear. Because isotropy is lost, spatial filtering in wall-bounded flows is not as straightforward as it is in HIT. As the channel is populated with long-living elongated streaks that span the entire periodic domain, filtering flow quantities in the x direction needs many independent realizations for convergence. Limited by the number of DNS samples, the streamwise wall-shear stress is low-pass filtered in the spanwise direction only. Filtering in the streamwise direction leads to less converged data and limits the analysis to small $|p|$ values. However, similar observations can still be made and none of the conclusions here are affected if the wall-shear stress is filtered in the streamwise direction. Figure 5(a) shows $\langle\exp(p\tau'_l)\rangle$ for $p = -4$, -3, 1, 1.5 as functions of the filtering length. Power-law behaviour is found in the enclosed region between $l^+ \approx 350$ and $l/\delta = 0.8$, thus providing direct support to (3.2). The bounds of the power-law scalings in flat-plate boundary layer flows are expected to be flow-dependent but not Reynolds-number-dependent (see e.g. de Silva *et al.* 2015). In flows where the wall is curved, the length scale imposed by the surface curvature l_R might limit the size of the attached eddies, thus limiting the range of the scalings to $\sim O(l_R)$.

The power-law scalings shown in figure 5(a) are often referred to as 'strong self-similarity'. The existence of 'strong self-similarity' depends on firstly the multifractal formalism, equation (3.2), and secondly the additives being i.i.d. As the addends are only i.i.d. in the log-region, 'strong self-similarity' can only be observed in the log-region and the corresponding range of spanwise scales, assuming that the momentum carrying eddies have an average spanwise-to-wall-normal aspect ratio 2–3 (Del Álamo *et al.* 2006; Lozano-Durán *et al.* 2012). Even supposing that the low-pass filtered streamwise stress fluctuation does follow an additive process across all scales, the addends of eddies in the bulk and the viscosity-affected regions are not expected to be statistically similar to those in the log-region. As a result, 'strong self-similarity' fails at viscosity-affected scales ($l^+ \lesssim 300$) and at integral scales ($l \sim O(\delta)$). At these scales, the multifractal formalism may be examined
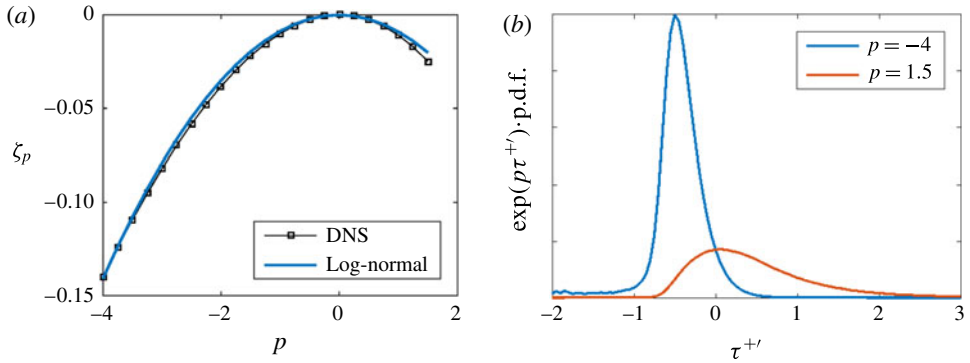
FIGURE 6. (*a*) Anomalous exponent as a function of the power exponent p. The solid line corresponds to $0.0098p^2$. (*b*) Premultiplied p.d.f. of $\exp(p\tau')$ for $p = -4$ and $p = 1.5$. The magnitude of the premultiplied p.d.f. is not relevant for the present work and is not shown here.

using the so-called extended self-similarity (ESS), which are power-law scalings of $\langle \exp(p\tau'_l) \rangle$ as functions of $\langle \exp(p_o\tau'_l) \rangle$ for fixed p_o. ESS does not depend critically on the addends being i.i.d. (see detailed discussion in Yang *et al.* 2016*c*), and therefore it is often referred to as 'weak self-similarity'. Figure 5(*b*) shows the ESS scalings for $p_o = -4$. In contrast to 'strong self-similarity', which is only found in the log-region, ESS scalings are found across all scales from $l^+ = 10$ to $l = \delta$. This suggests that the low-pass filtered streamwise stress fluctuations may be modelled using (3.2) across all scales, although the large-scale flow motions and the viscosity affect the statistical properties of the addends in the bulk region and the near-wall region, respectively.

ESS provides a measure of ζ_p/ζ_{p_o}. Therefore, the anomalous exponent ζ_p is known given a ζ_{p_o} (Benzi *et al.* 1993). While HIT admits an exact scaling $\langle \epsilon_n \rangle \sim \langle \epsilon \rangle$, the same is not true for the momentum cascade counterpart (except for the trivial case of $p = 0$, $\langle \exp(0 \cdot \tau_l) \rangle = 1$). As a result, the analogous anomalous exponent defined in (3.5) needs to be measured directly by fitting the data in the enclosed region in figure 5(*a*). The measured exponent ζ_p is shown as a function of the power exponent p in figure 6(*a*), which, according to the multifractal formalism, $\zeta_p = \log_2(\langle \exp(pa) \rangle)$. The anomalous exponent ζ_p was defined for the MGF of the streamwise velocity fluctuation (Yang, Marusic & Meneveau 2016*b*), which was subsequently found to be universal (Krug *et al.* 2017). While the universality of the anomalous exponent defined here has not been tested, it is likely that ζ_p for the wall-shear stress is also universal. It should be noted that without invoking the multifractal assumption, a is a constant, and ζ_p is a linear function of p. Following Kolmogorov (1962), and modelling the addends a as Gaussian random variables, it is straightforward to show that $\zeta_p = C_{LN}p^2$, where C_{LN} is a constant. As is seen, $C_{LN} = 0.0089$ gives a fairly good fit for the measured exponents. Because rare events are not fully accounted for in a log-normal model (Landau & Lifshitz 1987), the fact that log-normal model fits the measurements well suggests that the momentum cascade is less intermittent than the energy cascade counterpart.

Finally, the data convergence can be examined using the premultiplied probability density function (p.d.f.). Figure 6(*b*) shows the premultiplied p.d.f.s of $\exp(p\tau')$ for $p = -4$ and 1.5. Because $\exp(p\tau')$ emphasizes fluctuations that have the same sign as p, $\langle \exp(p_1\tau') \rangle$ converges more slowly than $\langle \exp(p_2\tau') \rangle$ for $|p_1| > |p_2|$, $p_1p_2 > 0$.

Also, because low-pass filtering damps fluctuations in a signal, $\langle\exp(p\tau')\rangle$ converges more slowly than $\langle\exp(p\tau'_l)\rangle$ (see O'Neil & Meneveau (1993), Yang *et al.* (2016*b*) for detailed discussion). As $\langle\exp(p\tau'_l)\rangle$ is the area under the its premultiplied p.d.f., figure 6(*b*) suggests that both $\langle\exp(-4\tau')\rangle$ and $\langle\exp(1.5\tau')\rangle$ are statistically converged. Then, by the reasoning above, all the statistics shown in figure 5(*a*) are converged. Limited by the number of DNS samples, statistics for $p < -4$ and $p > 1.5$ are poorly converged and therefore are not reported here.

4. Discussion and summary

In the present work, we have argued that the momentum cascade in wall-bounded turbulence is analogous to the energy cascade in HIT, and that it can be modelled as an additive process within the multifractal formalism. Analogous to the coarse-grained dissipation rates, the statistics associated to the exponential of the coarse-grained wall stresses follows power-law scalings. This leads to a new prediction for the variance of the wall-shear stress, that should scale as $\log(Re_\tau)$, in contrast to previous works, where the prediction holds for the standard deviation instead (Schlatter & Örlü 2010). In addition, we have shown that the wall stress satisfies reasonably well the 'strong self-similarity' hypothesis for scales spanning along the log-layer, and that the 'extended self-similarity' holds at all scales.

Despite the similarities between the energy and momentum cascades, there are many features in the former that are not present in the latter. (1) While the flow is roughly isotropic in the inertial range, the momentum cascade is hardly isotropic due to the effect of the shear. (2) The momentum cascade follows fairly well an additive process but the energy cascade is better represented by a multiplicative one. (3) Because τ' is not positive definite, back-scattering is allowed at dissipative scales in the momentum cascade but energy back-scattering hardly happens close to the dissipative scales. The consequence of this last point is that subgrid scale (SGS) modelling of the momentum cascade (in today's term, LES wall modelling, see e.g. Piomelli & Balaras (2002)) is probably more challenging than the conventional eddy-viscosity SGS modelling formulated in terms of the dissipation (Meneveau & Katz 2000). (4) Velocities at the wall, because of the non-slip condition, equal the velocity of the wall, making it difficult to formulate the momentum cascade using a Lagrangian frame of reference, which has shown to be quite successful in SGS modelling (Meneveau, Lund & Cabot 1996). In this sense, the results presented here might be a useful tool for LES wall modelling of many problems, where not only the mean stress but also the fluctuations are of interest. In this context, it is worth noting that currently available LES wall models underpredict wall-shear stress fluctuations (Park & Moin 2016) and the present work can be used to augment the subgrid stresses that are not resolved by the LES grids. (5) The anomalous exponent in the momentum cascade may be modelled as a parabolic function of the power exponent p, whereas in the energy cascade, a super-Gaussian model has to be employed. This suggests that the momentum cascade is less dominated by extreme events and hence is not as intermittent as the energy cascade.

Finally, despite the knowledge gained on the energy cascade in the past century and the analogy made here, the interscale transfer of momentum is still a problem of its own merits and much work remains to be done to fully understand this flow phenomenon.

Acknowledgements

References

ALFREDSSON, P. H., JOHANSSON, A. V., HARITONIDIS, J. H. & ECKELMANN, H. 1988 The fluctuating wall-shear stress and the velocity field in the viscous sublayer. *Phys. Fluids* **31** (5), 1026–1033.

AOYAMA, T., ISHIHARA, T., KANEDA, Y., YOKOKAWA, M. & UNO, A. 2005 Statistics of energy transfer in high-resolution direct numerical simulation of turbulence in a periodic box. *J. Phys. Soc. Japan* **74**, 3202–3212.

BAARS, W. J., HUTCHINS, N. & MARUSIC, I. 2017 Reynolds number trend of hierarchies and scale interactions in turbulent boundary layers. *Phil. Trans. R. Soc. Lond.* **375**, 2089.

BATCHELOR, G. K. 1953 *The Theory of Homogeneous Turbulence*. Cambridge University Press.

BENZI, R., CILIBERTO, S., TRIPICCIONE, R., BAUDET, C., MASSAIOLI, F. & SUCCI, S. 1993 Extended self-similarity in turbulent flows. *Phys. Rev.* E **48** (1), R29.

BIFERALE, L. 2003 Shell models of energy cascade in turbulence. *Annu. Rev. Fluid Mech.* **35** (1), 441–468.

CARDESA, J. I., VELA-MARTÍN, A., DONG, S. & JIMÉNEZ, J. 2015 The temporal evolution of the energy flux across scales in homogeneous turbulence. *Phys. Fluids* **27** (11), 111702.

DEL ÁLAMO, J. C., JIMENEZ, J., ZANDONADE, P. & MOSER, R. D. 2006 Self-similar vortex clusters in the turbulent logarithmic region. *J. Fluid Mech.* **561**, 329–358.

FLORES, O. & JIMÉNEZ, J. 2010 Hierarchy of minimal flow units in the logarithmic layer. *Phys. Fluids* **22** (7), 071704.

FRISCH, U. & DONNELLY, R. J. 1996 *Turbulence: The Legacy of AN Kolmogorov*. AIP.

FRISCH, U., SULEM, P.-L. & NELKIN, M. 1978 A simple dynamical model of intermittent fully developed turbulence. *J. Fluid Mech.* **87** (04), 719–736.

GOTO, S. 2012 Coherent structures and energy cascade in homogeneous turbulence. *Progress of Theoretical Physics Supplement* **195**, 139–156.

HEISENBERG, W. 1985 On the theory of statistical and isotropic turbulence. In *Original Scientific Papers Wissenschaftliche Originalarbeiten*, pp. 115–119. Springer.

JIMÉNEZ, J. 2012 Cascades in wall-bounded turbulence. *Annu. Rev. Fluid Mech.* **44**, 27–45.

JIMÉNEZ, J. 2016 Optimal fluxes and Reynolds stresses. arXiv:1606.02160.

KIM, J., MOIN, P. & MOSER, R. 1987 Turbulence statistics in fully developed channel flow at low Reynolds number. *J. Fluid Mech.* **177**, 133–166.

KOLMOGOROV, A. N. 1941 The local structure of turbulence in incompressible viscous fluid for very large Reynolds numbers. *Dokl. Akad. Nauk SSSR* **30**, 301–305.

KOLMOGOROV, A. N. 1962 A refinement of previous hypotheses concerning the local structure of turbulence in a viscous incompressible fluid at high Reynolds number. *J. Fluid Mech.* **13** (01), 82–85.

KRAICHNAN, R. H. 1965 Lagrangian-history closure approximation for turbulence. *Phys. Fluids* **8** (4), 575–598.

KRAICHNAN, R. H. 1991 Stochastic modeling of isotropic turbulence. In *New Perspectives in Turbulence*, pp. 1–54. Springer.

KRUG, D., YANG, X. I. A., DE SILVA, C. M., OSTILLA-MONICO, R., VERZICCO, R., MARUSIC, I. & LOHSE, D. 2017 Statistics of turbulence in the energy-containing range of Taylor–Couette compared to canonical wall-bounded flows. *J. Fluid Mech.* (submitted).

LANDAU, L. & LIFSHITZ, E. 1987 Fluid mechanics. In *Course of Theoretical Physics*. Pergamon.

LEE, M. & MOSER, R. D. 2015 Direct numerical simulation of turbulent channel flow up to $Re_\tau \approx$ 5200. *J. Fluid Mech.* **774**, 395–415.

LEITH, C. E. 1967 Diffusion approximation to inertial energy transfer in isotropic turbulence. *Phys. Fluids* **10**, 1409–1416.

LEUNG, T., SWAMINATHAN, N. & DAVIDSON, P. 2012 Geometry and interaction of structures in homogeneous isotropic turbulence. *J. Fluid Mech.* **710**, 453–481.

LOZANO-DURÁN, A., FLORES, O. & JIMÉNEZ, J. 2012 The three-dimensional structure of momentum transfer in turbulent channels. *J. Fluid Mech.* **694**, 100–130.

LOZANO-DURÁN, A., HOLZNER, M. & JIMÉNEZ, J. 2016 Multiscale analysis of the topological invariants in the logarithmic region of turbulent channels at a friction Reynolds number of 932. *J. Fluid Mech.* **803**, 356–394.

LOZANO-DURÁN, A. & JIMÉNEZ, J. 2014a Effect of the computational domain on direct simulations of turbulent channels up to $Re_\tau = 4200$. *Phys. Fluids* **26** (1), 011702.

LOZANO-DURÁN, A. & JIMÉNEZ, J. 2014b Time-resolved evolution of coherent structures in turbulent channels: characterization of eddies and cascades. *J. Fluid Mech.* **759**, 432–471.

MANDELBROT, B. B. 1972 Possible refinement of the lognormal hypothesis concerning the distribution of energy dissipation in intermittent turbulence. In *Statistical Models and Turbulence*, pp. 333–351. Springer.

MANDELBROT, B. B. 1999 Intermittent turbulence in self-similar cascades: divergence of high moments and dimension of the carrier. In *Multifractals and Noise*, pp. 317–357. Springer.

MARUSIC, I., MONTY, J. P., HULTMARK, M. & SMITS, A. J. 2013 On the logarithmic region in wall turbulence. *J. Fluid Mech.* **716**, R3.

MARUSIC, I. & PERRY, A. 1995 A wall-wake model for the turbulence structure of boundary layers. Part 2. Further experimental support. *J. Fluid Mech.* **298**, 389–407.

MATHIS, R., MARUSIC, I., CHERNYSHENKO, S. I. & HUTCHINS, N. 2013 Estimating wall-shear-stress fluctuations given an outer region input. *J. Fluid Mech.* **715**, 163–180.

MENEVEAU, C. & KATZ, J. 2000 Scale-invariance and turbulence models for large-eddy simulation. *Annu. Rev. Fluid Mech.* **32** (1), 1–32.

MENEVEAU, C., LUND, T. S. & CABOT, W. H. 1996 A Lagrangian dynamic subgrid-scale model of turbulence. *J. Fluid Mech.* **319**, 353–385.

MENEVEAU, C. & SREENIVASAN, K. 1987 Simple multifractal cascade model for fully developed turbulence. *Phys. Rev. Lett.* **59** (13), 1424–1427.

MENEVEAU, C. & SREENIVASAN, K. 1991 The multifractal nature of turbulent energy dissipation. *J. Fluid Mech.* **224**, 429–484.

MORRILL-WINTER, C., PHILIP, J. & KLEWICKI, J. 2017 Statistical evidence of anasymptotic geometric structure to the momentum transporting motions in turbulent boundary layers. *Phil. Trans. R. Soc. Lond.* A **375** (2089), 20160084.

OBUKHOV, A. M. 1941 On the distribution of energy in the spectrum of turbulent flow. *Izv. Akad. Nauk SSSR Geogr. Geofiz.* **5** (4), 453–466.

O'NEIL, J. & MENEVEAU, C. 1993 Spatial correlations in turbulence: predictions from the multifractal formalism and comparison with experiments. *Phys. Fluids* A **5** (1), 158–172.

ONSAGER, L. 1949 Statistical hydrodynamics. *Il Nuovo Cimento* **6**, 279–287.

ORSZAG, S. A. 1970 Analytical theories of turbulence. *J. Fluid Mech.* **41**, 363–386.

ÖSTERLUND, J. M. 1999 *Experimental Studies of Zero Pressure-Gradient Turbulent Boundary Layer Flow*. Royal Institute of Technology, Department of Mechanics.

PARK, G. I. & MOIN, P. 2016 Space-time characteristics of wall-pressure and wall shear-stress fluctuations in wall-modeled large eddy simulation. *Phys. Rev. Fluids* **1** (2), 024404.

PARK, G. I., WALLACE, J. M., WU, X. & MOIN, P. 2012 Boundary layer turbulence in transitional and developed states. *Phys. Fluids* **24** (3), 035105.

PERRY, A. E. & CHONG, M. S. 1982 On the mechanism of wall turbulence. *J. Fluid Mech.* **119**, 173–217.

PIOMELLI, U. & BALARAS, E. 2002 Wall-layer models for large-eddy simulations. *Annu. Rev. Fluid Mech.* **34** (1), 349–374.

PIOMELLI, U., CABOT, W. H., MOIN, P. & LEE, S. 1991 Subgrid-scale backscatter in turbulent and transitional flows. *Phys. Fluids* A **3** (7), 1766–1771.

POPE, S. B. 2001 *Turbulent Flows*. IOP Publishing.

RICHARDSON, L. F. 1922 *Weather Prediction by Numerical Process*. Cambridge University Press.

SADDOUGHI, S. G. & VEERAVALLI, S. V. 1994 Local isotropy in turbulent boundary layers at high Reynolds number. *J. Fluid Mech.* **268**, 333–372.

SCHLATTER, P. & ÖRLÜ, R. 2010 Assessment of direct numerical simulation data of turbulent boundary layers. *J. Fluid Mech.* **659**, 116–126.

DE SILVA, C., MARUSIC, I., WOODCOCK, J. & MENEVEAU, C. 2015 Scaling of second-and higher-order structure functions in turbulent boundary layers. *J. Fluid Mech.* **769**, 654–686.

TOWNSEND, A. A. 1980 *The Structure of Turbulent Shear Flow*. Cambridge University Press.

VINUESA, R., DUNCAN, R. D. & NAGIB, H. M. 2016 Alternative interpretation of the superpipe data and motivation for ciclope: the effect of a decreasing viscous length scale. *Eur. J. Mech.* *(B/Fluids)* **58**, 109–116.

YANG, X. I. A., MARUSIC, I. & MENEVEAU, C. 2016*a* Hierarchical random additive process and logarithmic scaling of generalized high order, two-point correlations in turbulent boundary layer flow. *Phys. Rev. Fluids* **1** (2), 024402.

YANG, X. I. A., MARUSIC, I. & MENEVEAU, C. 2016*b* Moment generating functions and scaling laws in the inertial layer of turbulent wall-bounded flows. *J. Fluid Mech.* **791**, R2.

YANG, X. I. A., MENEVEAU, C., MARUSIC, I. & BIFERALE, L. 2016*c* Extended self-similarity in moment-generating-functions in wall-bounded turbulence at high Reynolds number. *Phys. Rev. Fluids* **1** (4), 044405.